Scripta Materialia 112 (2016) 79–82

Contents lists available at ScienceDirect

Scripta Materialia

journal homepage: www.elsevier.com/locate/scriptamat

Time-dependent nanoscale plasticity in nanocrystalline nickel rods and tubes

Jung-A Lee [a], Brandon B. Seo [b], In-Chul Choi [a], Moo-Young Seok [a], Yakai Zhao [a], Zeinab Jahed [b], Upadrasta Ramamurty [c,d], Ting Y. Tsui [b,e,*], Jae-il Jang [a,**]

[a] Division of Materials Science and Engineering, Hanyang University, Seoul 133-791, South Korea
[b] Department of Mechanical Engineering, University of Waterloo, Waterloo, ON N21 3G1, Canada
[c] Department of Materials Engineering, Indian Institute of Science, Bangalore 560012, India
[d] Center of Excellence for Advanced Materials Research, King Abdulaziz University, Jeddah 21589, Saudi Arabia
[e] Waterloo Institute of Technology, University of Waterloo, Waterloo, ON N21 3G1, Canada

ARTICLE INFO

Article history:
Received 7 August 2015
Received in revised form 8 September 2015
Accepted 8 September 2015
Available online 20 September 2015

Keywords:
Nanocrystalline Ni
Time-dependent plasticity
Microcompression
Creep
Strain-rate sensitivity

ABSTRACT

Time-dependent nanoscale plasticity of nanocrystalline nickel at room temperature was critically explored through a series of micropillar creep and quasi-static compression experiments on rod and tube specimens fabricated by electron beam lithography and electroplating. Enhanced creep rates in tubes as compared to rods, establishes the facilitating role played by the free surface in time-dependent deformation. Creep stress exponent, n, and strain-rate sensitivity, m, were compared to examine connections between creep and the rate-dependent plasticity, if any.

Plastic deformation in nanocrystalline (nc) metals and alloys (with a grain size $d < 100$ nm) is a topic of current and active research, with most recent focus on the mechanical behavior of small-scale nc samples through micro-/nano-pillar testing [1–11], especially of metals with face-centered cubic crystal structure (Ni [2–7], Cu [8,9], Pt [10], and Rh [11]). In these studies, the effects of sample size on the yield strength and flow stress were explored [3–5,9,10]. Results of one study [3] indicate that "smaller is stronger" which is similar to that typically observed in the pillars of single crystal or coarse-grained metals [12–14]. A number of other studies (e.g., for the pillars of Ni–W ($d \sim 60$ nm) [4], Ni ($d \sim 12$ nm) [5], Cu ($d \sim 100$ nm) [9], and Pt ($d \sim 12$ nm) [10]) suggest an opposite trend, i.e., "smaller is weaker." Although the mechanism for this size-dependent weakening of the nc pillars has not been understood in detail yet, it was thought to be related to the role of free surfaces. For instance, Jang and Greer [4] postulated that a free surface can enhance grain boundary (GB)-mediated deformation process in Ni–W pillars structures.

Recently, the time-dependent plasticity at room temperature (RT) of nc pillars was also researched [6,7]. Choi et al. [6] observed creep deformation at RT of a series of nc Ni pillars having different pillar diameter D and revealed that the creep gets more pronounced as D gets smaller, and suggested that the increased surface-to-volume ratio (SVR) with decreasing D is possibly the reason behind this observation. However, the precise connection between change in SVR and sample size effect requires critical investigation, as simply changing the deforming volume (irrespective of the roles of surfaces) can also bring about out other changes in metallurgical and mechanical environments. One such example is that when the sample volume is changed, the size and distribution of defects that affect the mechanical behavior also change. To address this, which is the first motive of this study, we employ nc pillars with the same outer D but with substantially different SVR and perform creep experiments. The second objective of this study is to establish a quantitative relation between creep and rate-dependency of flow stress in terms of the material parameter that governs each of these phenomena; i.e., the stress exponent $n(=(\frac{\partial \ln \dot{\varepsilon}}{\partial \ln \sigma})_{\sigma,T})$ for creep and strain-rate sensitivity $m(=(\frac{\partial \ln \sigma}{\partial \ln \dot{\varepsilon}})_{\dot{\varepsilon},T})$ for rate-dependency of flow stress. Due to the similarity in the mathematical description of these material constants, n is often estimated from m (which is obtained from the quasi-static uniaxial tests conducted at various strain rates) or vice versa, by simple conversion, viz. $n = 1/m$ [15–18]. Nevertheless, the appropriateness of this conversion for nc pillars has not been systematically examined yet. This may be due to the difficulties in conducting meaningful constant strain-rate pillar compression tests in

* Corresponding author at: Department of Mechanical Engineering, University of Waterloo, Waterloo, ON N21 3G1, Canada.
** Corresponding author at: Division of Materials Science and Engineering, Hanyang University, Seoul 133-791, South Korea.
E-mail addresses: tttsui@uwaterloo.ca (T.Y. Tsui), jijang@hanyang.ac.kr (J-i. Jang).

http://dx.doi.org/10.1016/j.scriptamat.2015.09.017
1359-6462/

large numbers, because the pillars are often prepared by focused ion beam (FIB) milling that requires much time and cost.

To address the above issues, here we performed a series of creep and constant strain-rate tests, both in uniaxial compression, on nc Ni pillars prepared through electroplating processes. There are three clear advantages in utilizing such pillars. First, it was possible to prepare pillars having different SVRs but the same outer D, such as rods and tubes with the same outer D. Second, we could produce several hundreds of pillars in single batch of process, which made it possible to conduct statistically significant large number of constant strain-rate tests. Third, we could avoid any possible surface effect induced during FIB milling process and thus related artifacts [19]. It is also noteworthy that pillar compression creep test is known to overcome the issues arising from nanoindentation creep test [20].

Two types of nc Ni pillars (including rods and tubes) were fabricated via electron beam lithography and electroplating process [19]. Silicon substrates covered with thin Ti (~20 nm) and Au (~20–60 nm) seed layers were spin coated with polymethylmethacrylate (PMMA) resist. Arrays of circular and ring-shaped via-holes were patterned in the PMMA using electron beam lithography. Subsequently, patterned PMMA molds were filled with nc Ni by electroplating. For electroplating, a commercial grade pure Ni was used as anode and the solution was made of Ni (II) sulfate hexahydrate (99%, Sigma Aldrich), Ni (II) chloride (98%, Sigma Aldrich), boric acid (BX0865, EMD Millipore), and organic additive saccharin (98%, Sigma Aldrich). After electroplating, the remaining PMMA resist was removed with acetone. A specific advantage of this technique is that strong sample uniformity across each substrate can be obtained through this FIB-less fabrication of pillars. Representative microstructure of the pillars was examined using transmission electron microscopy (TEM), JEM-2010F (JEOL Ltd., Tokyo, Japan).

Both quasi-static, constant strain-rate compression tests and constant-load creep tests of the pillars were performed at RT using Nanoindenter XP (formerly MTS; now Keysight Tech., Oak Ridge, TN) with a FIB-milled cylindrical diamond punch having a top diameter of ~14 um. During the creep tests under compressive loading, the load was increased up to the desired maximum stress level (i.e., 600, 800, 1000 MPa, respectively), then held for 1000 s, and finally removed at the same rate as the loading segment. During the quasi-static compression tests, the rods and tubes were loaded under strain rates ($\dot{\varepsilon}$) ranging from 0.0001 to 0.005/s. Pillar morphologies were imaged before and after the nanomechanical testing using scanning electron microscopy (SEM), JSM-6330F (JEOL Ltd., Tokyo, Japan). Additionally, in-situ compression tests were performed on rods inside a Quanta 250 FEG SEM (FEI Inc., Hillsboro, OR) using a PI 85 picoindenter (Hysitron Inc., Minneapolis, MN) at relatively high $\dot{\varepsilon}$ (0.002–0.01/s).

Fig. 1 exhibits representative SEM and TEM images showing the shapes and microstructures of as-fabricated pillars. The SEM micrographs reveal that pillar tops are flat and there is almost no taper between sidewalls and substrates. Nominal outer D and aspect ratio of both rods and tubes are ~1000 nm and ~1.7, respectively, and sidewall thickness of the tubes is ~175 nm. As shown in the high-resolution TEM image in Fig. 1, the average grain size d of rods was determined as ~12 nm. Although TEM observation of tubes was not performed here, similar microstructure was expected for tubes since tubes and rods were prepared on the same substrate and in the same solution [5].

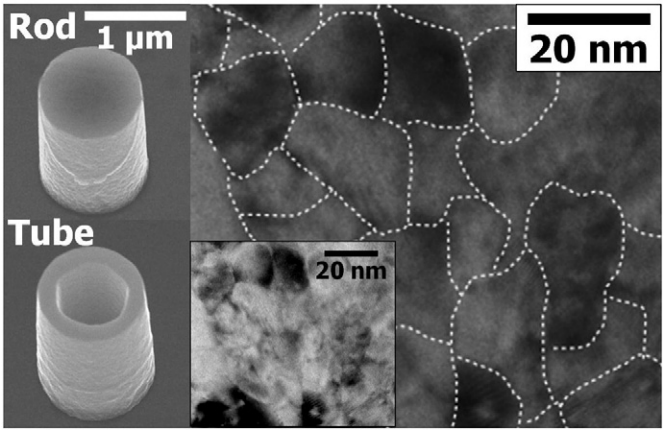

Fig. 1. Representative SEM and TEM images (with inset TEM image without dashed line) showing the geometry and grain structure of as-fabricated nc Ni pillars.

First, constant-load compressive creep tests were conducted on rods and tubes. From the load–displacement (P–h) curves recorded during the tests, engineering stress P/A_0 (where A_0 is the initial cross-sectional area of pillar) vs. engineering strain h/L_0 (where L_0 is the initial pillar height) plots was obtained, as shown in Fig. 2a. The level of the applied stress for the load-holding sequence (i.e., creep stress σ_{creep}) is within nominal elastic range, which manifests as superimposition of the loading portion in stress–strain curves. For both rods and tubes, the maximum value of creep strain generated during the hold segment (ε_{creep}) increases obviously with σ_{creep}. This stress-dependency of the maximum ε_{creep} supports that the observed creep behavior is not an artifact caused by thermal drift which cannot depend on the level of applied load (and thus σ_{creep}) [21]. Variation of ε_{creep} with the hold time (t_{hold}) curves (for σ_{creep} = 1000 MPa) is provided in the inset of Fig. 2b. These creep curves apparently consist of two regimes in the early stages: primary (transient) creep regime and secondary creep regime where the apparent ε_{creep} vs. $t_{holding}$ relation shows a higher linearity. This two-regime behavior also supports that the creep observed in this study is not caused by thermal drift, because thermal drift is not expected to induce this two-regime curves [6]. As shown in the figure, at a given σ_{creep}, ε_{creep} obtained on tubes was always higher

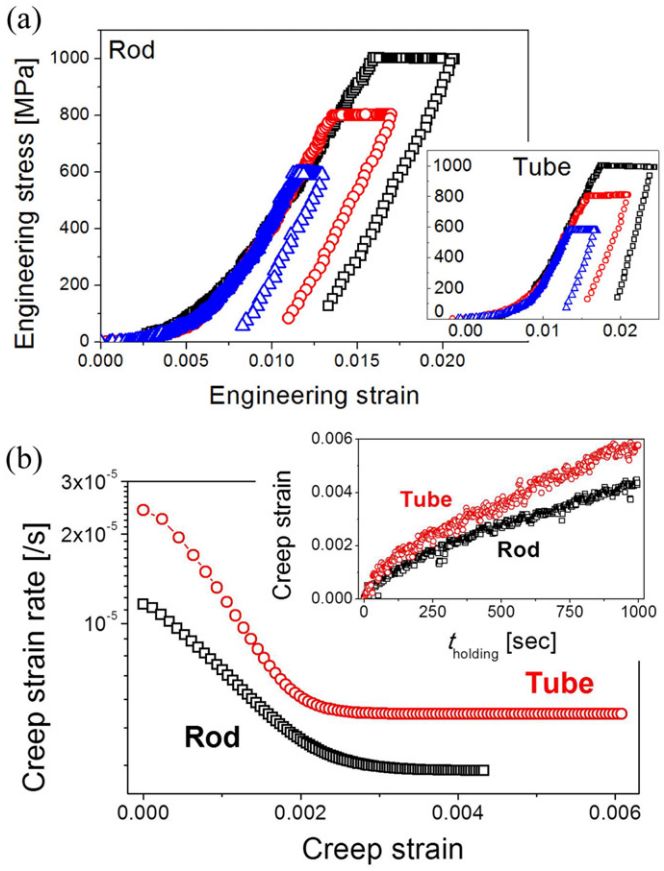

Fig. 2. Results of creep tests: (a) Representative stress–strain curves from creep tests; (b) example (for σ_{creep} = 1 GPa) of the logarithmic creep strain rate vs. creep strain relation (with inset plot of creep strain vs. holding time).

than that on rods, implying that creep deformation is more pronounced in tubes than in rods. Two-regime behavior is clearly seen in the main plot of Fig. 2b showing typical example (for $\sigma_{creep} = 1000$ MPa) of creep strain rate ($\dot{\varepsilon}_{creep}$) vs. ε_{creep}. To estimate $\dot{\varepsilon}_{creep}$, ε_{creep} vs. t_{hold} curves (inset of Fig. 2b) were fitted according to Garofalo's equation, $\varepsilon_{creep} = \alpha[1 - \exp(-rt_{hold})] + \omega t_{hold}$ (where α, ω, and r are creep constants) [6], which are then differentiated with respect to t_{hold}. As shown in Fig. 2b, the variation in $\dot{\varepsilon}_{creep}$ with ε_{creep} (which reflects the steady-state more accurately than $\dot{\varepsilon}_{creep}$ vs. t_{hold}) suggests the possibility of close approach to the steady-state condition (hereafter called 'quasi-steady-state, QSS'). It is noteworthy that in both primary and secondary (QSS) regimes, tubes always show higher $\dot{\varepsilon}_{creep}$ than rods at a given ε_{creep}.

From the above results, it is apparent that creep deformation is more pronounced in tubes (i.e., larger values of ε_{creep} and $\dot{\varepsilon}_{creep}$) than in rods. This strongly supports the purported scenario that free surfaces indeed have a major role to play in the creep deformation of nanostructures because the nominal SVR for the tubes (0.0129/nm) is three times higher than that of the rods (0.0045/nm). Possible mechanisms for the contribution of free surface to the enhanced creep behavior can be categorized into three groups. In first two mechanisms, role of free surface (that may be applicable to the creep in pillars of any type of material including single-crystal/poly-crystalline/non-crystalline material, not limited to nanocrystalline metals) is a strong diffusion path [6,21,22]. Note that the diffusivity of Ni along a free surface is 240 times higher than that along GB [6]. This surface-enhanced diffusivity can contribute to the increased creep in two ways. One is a direct way via diffusion creep mechanism; i.e. the creep can be significantly enhanced by vacancy/mass diffusion along surface. The other, and indirect way, is by enhanced dislocation activity. That is, assisted by prior diffusion process, free surfaces may act as sources for dislocation nucleation [23,24]. This possibility was supported by recent observation that activation volume for surface dislocation nucleation is small and is comparable to that for diffusion process [23,25]. In the third possible mechanism, the role of free surface can be envisioned simply as a relaxer of the mechanical constraints within pillars [26]. This, in turn, can result in more pronounced GB-mediated deformation of nc metals (including GB sliding or grain rotation) near free surface [10,27]. Details about the relative amounts of contribution from each of the aforementioned mechanisms require further investigation.

In order to address the second issue of the relation between n and m (i.e., "is simple conversion $n = 1/m$ proper?"), quasi-static, constant strain-rate compression tests up to a large plastic strain were conducted on rods and tubes. From P-h curves, the values of true (flow) stress (σ_f) and true strain (ε) in plastic regime were calculated according to $\sigma_f = \frac{P}{A} \sim \frac{PL}{A_0 L_0}$ and $\varepsilon = \ln(\frac{L}{L_0})$ where A and L are the instantaneous cross-sectional area and height of pillars, respectively. Typical stress–strain curve obtained on a rod, which was strained up to ~130% at $\dot{\varepsilon} = 0.01/s$, is shown in Fig. 3a. Similar behavior was observed in tubes (not shown here). Typical SEM micrographs of rods/tubes strained to the maximum capacity are presented in the insets of Fig. 3a; large plasticity can be noted in both of them, i.e., they were plastically deformed until they become pan-cake-shaped. While superplasticity of metallic materials under tensile stress is generally observed at both low $\dot{\varepsilon}$ ($10^{-5} - 10^{-4}$/s) and high temperatures (>$0.5T_m$ where T_m is the melting temperature), in this study, superplastic-like deformation under compression is obtained at relatively high $\dot{\varepsilon}$ ($10^{-3} - 10^{-1}$/s) and at room temperature (~$0.17T_m$ where T_m is the melting temperature of Ni; 1726 K). Especially, barreling, which is typically observed during compression tests was not observed. Supplementary material provides a movie taken from in-situ experiments showing the superplastic-like behavior of a rod at $\dot{\varepsilon} = 0.01/s$. Note that, in high-temperature deformation behavior of conventional coarse-grained metals, creep and superplastic deformation are closely related to each other in terms of deformation mechanisms. Therefore, one may imagine

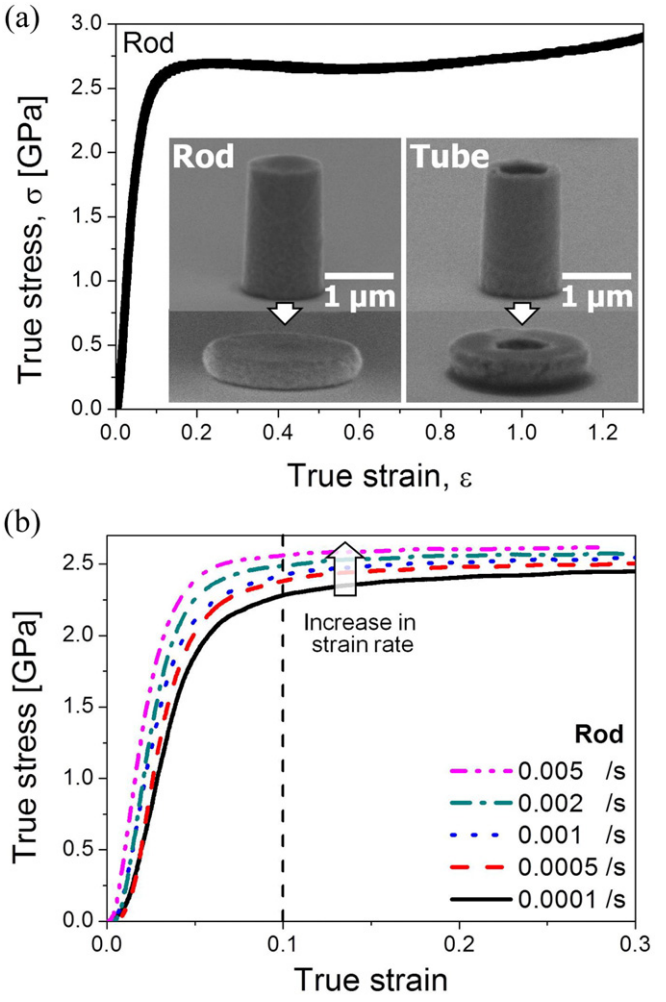

Fig. 3. Results of compression tests: (a) Typical stress–strain curve of rod recorded during compression up to the maximum capacity (with inset images showing SEM micrographs of a rod and tube taken before and after test); (b) variation in stress–strain curves of rod with varying applied strain rates.

that the above superplastic-like behavior at room temperature can be directly related to the creep behavior.

To estimate m value that often characterizes the superplasticity in tension [28], a series of constant strain-rate compression tests were performed at various $\dot{\varepsilon}$ (ranging from 0.0001/s to 0.005/s). Fig. 3b provides a set of σ_f-ε curves of rods obtained at various $\dot{\varepsilon}$. There is a significant rate dependency on σ_f; i.e., at any given ε, σ_f increases with $\dot{\varepsilon}$ (which was the same for tubes although not shown here). Variations in σ_f with $\dot{\varepsilon}$ (at $\varepsilon = 0.1$) are summarized in Fig. 4a. From the slope of the line in a logarithmic plot of σ_f vs. $\dot{\varepsilon}$, m was calculated as ~0.021 for rods and ~0.034 for tubes. Two points are noteworthy. First, the obtained value of m for rods falls within the range of data (~0.01–0.03) reported in literature through tensile tests on bulk nc metals [29–32], which is reasonable considering the micron size of the rods tested here and the difference between tension and compression. Second, although these values are much lower than that from traditional superplastic materials, viz. 0.4–0.8 [33], superplastic-like deformation under compressive stress (as in this study) does not necessarily require a high m because necking does not occur under compression [34]. An important feature in Fig. 4a is that tubes exhibit higher m than rods, which also supports the earlier observation made in this study that the SVR affects time-dependent plastic deformation behavior. By $n = 1/m$, representative m value can be converted into n of ~48 and ~29 for rods and tubes

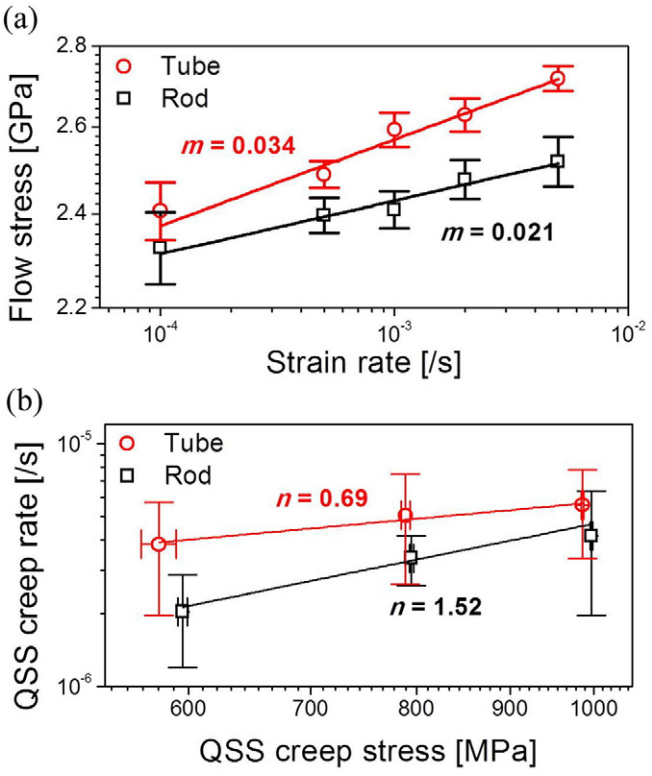

Fig. 4. Determination of two main parameters for the time-dependent plasticity: (a) m values estimated from flow stress vs. strain rate relation; (b) n values estimated from QSS creep strain rate vs. QSS creep stress relation.

respectively. These values are unreasonably high and physically implausible for creep behavior.

To directly obtain the n values from creep data, the QSS creep rate ($\dot{\varepsilon}_{QSS}$) was determined from the $\dot{\varepsilon}_{creep}$ value at $t_{holding} = 1000$ s. The variations in $\dot{\varepsilon}_{QSS}$ with the stress corresponding to QSS creep (σ_{QSS}) for both pillars are summarized in Fig. 4b. Since stress continuously varies during the constant-load creep test performed in this study, the σ_{QSS} was determined as the stress at $t_{hold} = 1000$ s; this is why σ_{QSS} in Fig. 4b is not exactly the same for tubes and rods. Then, n is estimated from the slope of logarithmic $\dot{\varepsilon}_{QSS}$ and σ_{QSS} plot. From linear fitting of the average points in Fig. 4b, n was determined as ~1.5 for rods and ~0.7 for tubes. It is well accepted that n is a useful indicator for deducing the dominant creep mechanism; i.e., $n = 1$ for diffusion creep such as Nabarro–Herring creep (by lattice diffusion) and Coble creep (by GB diffusion), $n = 2$ for GB sliding, and $n = 3$–8 for dislocation creep [28]. Although the estimated n values showed some fluctuations because they are from only average points, the n values for both rod and tube are below ~2, which means predominant mechanism is surface/GB mediated deformation (including diffusion along both paths and GB sliding). Even when the fluctuation in the estimated n values is considered, it is clear that tubes have lower n than rods, which also supports the notion that the free surfaces aid in the time-dependent plasticity.

The significant divergence between experimentally-measured n values (0.69 for rods and 1.52 for tubes) and those estimated by inverting m can be rationalized as following: Choi et al. [6] suggested the differences in the type of loading between compressive creep experiments and quasi-static compression tests as a possible reason for such large difference. While n is determined by measuring the change in strain at a given stress (and temperature), m is estimated by the change in stress at a given strain (and temperature). More importantly, there is a significant difference in applied stress level and $\dot{\varepsilon}$ range. The conventional creep tests are usually carried out well below the yield strength of the material being examined, but the stress used for determining m is plastic flow stress. In analogy, $\dot{\varepsilon}_{creep}$ in creep tests and $\dot{\varepsilon}$ for compression tests are in the completely different range; $\dot{\varepsilon}$ is 100–1000 times higher than $\dot{\varepsilon}_{creep}$, which can bring out different deformation mechanism. For instance, the diffusion-mediated process can be reduced with increasing in $\dot{\varepsilon}$ due to lack of the time for diffusion [17,18,35].

In summary, we have critically investigated the effect of surface-to-volume ratio on the creep and superplastic-like deformation at the nanoscale in a nc metal. Our results show that creep is enhanced in tubes as compared to rods of identical material and outer diameter, which clearly indicates that higher SVR indeed aids time-dependent deformation. Quantitative connections between creep and the rate-dependent plasticity were discussed by comparing the creep stress exponent n and strain-rate sensitivity m, which indicate that the simple conversion of $n = 1/m$, which is often used, does not hold, possibly because of the differences in the levels of applied stress and strain rate for extracting these properties as well as the way each of them are defined.

Acknowledgments

The work at Hanyang University was supported by the National Research Foundation of Korea (NRF) grant funded by Korea government (MSIP) (No. 2013R1A1A2A10058551). T.Y. Tsui thanks Natural Sciences and Engineering Research Council of Canada Discovery (Grant no. RGPIN-355552) and the Canada Foundation for Innovation (Project no. 18943) for the support on this research.

Appendix A. Supplementary data

Supplementary data to this article can be found online at http://dx.doi.org/10.1016/j.scriptamat.2015.09.017.

References

[1] J.R. Greer, J.T.M. De Hosson, Prog. Mater. Sci. 56 (2011) 654.
[2] B.E. Schuster, Q. Wei, H. Zhang, K.T. Ramesh, Appl. Phys. Lett. 88 (2006) 103112.
[3] A. Rinaldi, P. Peralta, C. Friesen, K. Sidradzki, Acta Mater. 56 (2008) 511.
[4] D. Jang, J.R. Greer, Scr. Mater. 64 (2011) 77.
[5] B.B. Seo, Z. Jahed, M.J. Burek, T.Y. Tsui, Mater. Sci. Eng. A 596 (2014) 275.
[6] I.-C. Choi, Y.-J. Kim, M.-Y. Seok, B.-G. Yoo, J.-Y. Kim, Y.M. Wang, J.-i. Jang, Int. J. Plast. 41 (2013) 53.
[7] G. Mohanty, J.M. Wheeler, R. Raghavan, J. Wehrs, M. Hasegawa, S. Mischler, L. Philippe, J. Michler, Philos. Mag. 95 (2015) 1878.
[8] D. Jang, C. Cai, J.R. Greer, Nano Lett. 11 (2011) 1743.
[9] N.L. Okamoto, D. Kashioka, T. Hirato, H. Inui, Int. J. Plast. 56 (2014) 173.
[10] X.W. Gu, C.N. Loynachan, Z. Wu, Y.-W. Zhang, D.J. Srolovitz, J.R. Greer, Nano Lett. 12 (2012) 6385.
[11] T.Y. Tsui, Z. Jahed, R.D. Evans, M.J. Burek, Philos. Mag. 95 (2015) 1751.
[12] M. Dietiker, S. Buzzi, G. Pigozzi, J.F. Löffler, R. Spolenak, Acta Mater. 59 (2011) 2180.
[13] D.M. Dimiduk, M.D. Uchic, T.A. Parthasarathy, Acta Mater. 53 (2005) 4065.
[14] J.R. Greer, W.C. Oliver, W.D. Nix, Acta Mater. 53 (2005) 1821.
[15] V. Maier, B. Merle, M. Goken, K. Durst, J. Mater. Res. 28 (2013) 1177.
[16] Y. Ma, G.J. Peng, D.H. Weng, T.H. Zhang, Mater. Sci. Eng. A 621 (2015) 111.
[17] G. Wang, J. Lian, Z. Jiang, L. Qin, Q. Jiang, J. Appl. Phys. 106 (2009) 086105.
[18] Z. Jiang, X. Liu, G. Li, Q. Jiang, J. Lian, Appl. Phys. Lett. 88 (2006) 143115.
[19] M.J. Burek, J.R. Greer, Nano Lett. 10 (2010) 69.
[20] I.-C. Choi, B.-G. Yoo, Y.-J. Kim, J.-i. Jang, J. Mater. Res. 27 (2012) 3.
[21] B.-G. Yoo, J.-Y. Kim, Y.-J. Kim, I.-C. Choi, S. Shim, T.S. Tsui, H. Bei, U. Ramamurty, J.-i. Jang, Int. J. Plast. 37 (2012) 108.
[22] Y.-J. Kim, W.W. Lee, I.-C. Choi, B.G. Yoo, S.M. Han, H.-G. Park, W.I. Park, J.-i. Jang, Acta Mater. 61 (2013) 7180.
[23] L.Y. Chen, M.-r. He, J. Shin, G. Richter, D.S. Gianola, Nat. Mater. 14 (2015) 707.
[24] J. Li, S. Sarkar, W. Cox, T.J. Lenosky, E. Bitzek, Phys. Rev. B 84 (2011) 054103.
[25] T. Zhu, J. Li, A. Samanta, A. Leach, K. Gall, Phys. Rev. Lett. 100 (2008) 025502.
[26] Z.X. Wu, Y.W. Zhang, M.H. Jhon, J.R. Greer, D.J. Srolovitz, Acta Mater. 61 (2013) 1831.
[27] D.S. Gianola, D. Farkas, M. Gamarra, M. He, J. Appl. Phys. 112 (2012) 124313.
[28] G.E. Dieter, Mechanical Metallurgy, McGraw-Hill, London, 1988.
[29] M. Dao, L. Lu, R.J. Asaro, J.T.M. De Hosson, E. Ma, Acta Mater. 55 (2007) 4041.
[30] S. Cheng, E. Ma, Y.M. Wang, L.J. Kecskes, K.M. Youssef, C.C. Koch, U.P. Trociewitz, K. Han, Acta Mater. 53 (2005) 1521.
[31] F. Dalla Torre, H. Van Swygenhoven, M. Victoria, Acta Mater. 50 (2002) 3957.
[32] Y.M. Wang, E. Ma, Appl. Phys. Lett. 85 (2004) 2750.
[33] A.H. Chokshi, A.K. Mukherjee, T.G. Langdon, Mater. Sci. Eng. R 10 (1993) 237.
[34] D. Pan, S. Kuwano, T. Fujita, M.W. Chen, Nano Lett. 7 (2007) 2108.
[35] J. Mu, Z. Jiang, W. Zheng, H. Tian, J. Lian, Q. Jiang, J. Appl. Phys. 111 (2012) 063506.